# Eukaryotic Chemotaxis under Periodic Stimulation Shows Temporal Gradient Dependence

Richa Karmakar,[†,‡] Aravind Karanam,[‡] Man-Ho Tang, and Wouter-Jan Rappel[*]
*Department of Physics, University of California, San Diego, La Jolla, California 92093, USA*

(Received 11 October 2023; accepted 8 July 2024; published 8 August 2024)

When cells of the social amoeba *Dictyostelium* discoideum are starved of nutrients they start to synthesize and secrete the chemical messenger and chemoattractant cyclic adenosine monophosphate (cAMP). This signal is relayed by other cells, resulting in the establishment of periodic waves. The cells aggregate through chemotaxis toward the center of these waves. We investigated the chemotactic response of individual cells to repeated exposure to waves of cAMP generated by a microfluidic device. For fast-moving waves (short period), the chemotactic ability of the cells was found to increase upon exposure to more waves, suggesting the development of a memory over several cycles. This effect was not significant for slow-moving waves (large period). We show that the experimental results are consistent with a local excitation global inhibition-based model, extended by including a component that rises and decays slowly and that is activated by the temporal gradient of cAMP concentration. The observed enhancement in chemotaxis is relevant to populations in the wild: once sustained, periodic waves of the chemoattractant are established, it is beneficial to cells to improve their chemotactic ability in order to reach the aggregation center sooner.

DOI: 10.1103/PhysRevLett.133.068401

Chemotaxis, the chemically guided motion of cells, is critical to several biological processes such as foraging, wound healing, embryonic development, and cancer metastasis [1–5]. The social amoeba *Dictyostelium* discoideum is a well-characterized model organism to study chemotaxis. It displays a unicellular to multicellular transition in its life cycle when starved of nutrients, by aggregating through chemotaxis [6,7], driven by the chemoattractant cyclic adenosine monophosphate (cAMP), a small molecule that is internally synthesized and secreted by the cells [8]. The multicellular aggregate then forms a stalk and a fruiting body, which contains spores that can later be dispersed [9,10].

During aggregation, *Dictyostelium* cells not only produce the chemoattractant but also relay the signal, resulting in cAMP waves that sweep through the population [11]. This signal-relay process is also present in other chemotactic systems [12,13] and ensures the recruitment of cells over large distances. Initially, the cAMP waves arise spontaneously from many locations in the population. As development continues, sources with high frequencies dominate and become stable aggregation centers [14]. Many models of the aggregation process have been proposed, ranging from qualitative excitable system models to more biochemically oriented ones [15–19]. In addition, modeling studies have been published that attempt to describe the chemotactic response of a single cell to chemoattractant gradients [20–22].

Traditionally, most experimental and modeling chemotaxis studies have focused on the response of cells to static gradients [23,24]. More recently, using microfluidic devices, it has become possible to expose cells to carefully controlled complex and time-varying gradients [25–30]. For example, it was shown that the levels of activated Ras, a precursor to actin polymerization, revert to prestimulus levels following a uniform abrupt rise in the external cAMP concentration, thereby showing perfect adaptation [31]. Also, experiments that generated chemoattractant waves of controlled speed have shown that cells can be more sensitive to the positive gradient in the incoming half of a wave and less sensitive to the negative gradient in the back half of the wave [32,33]. The extent of this biased cell motion has been shown to depend on the chemoattractant wave period [32,33] as well as the background concentration of the chemoattractant [30]. These studies also support the involvement of a local excitation global inhibition (LEGI) module in chemotaxis [32,33], in which the activated receptor produces both a membrane-bound localized activator and a globally diffusible inhibitor, with fast and slow kinetics, respectively [20,34].

A previous study showed that cells are insensitive to a falling cAMP concentration when exposed to a single chemoattractant wave [33]. It is not clear, however, how

[*]Contact author: rappel@physics.ucsd.edu
[†]Present address: Department of Biotechnology, Indian Institute of Technology Madras, Chennai 600036, India.
[‡]These authors contributed equally to this work.

 

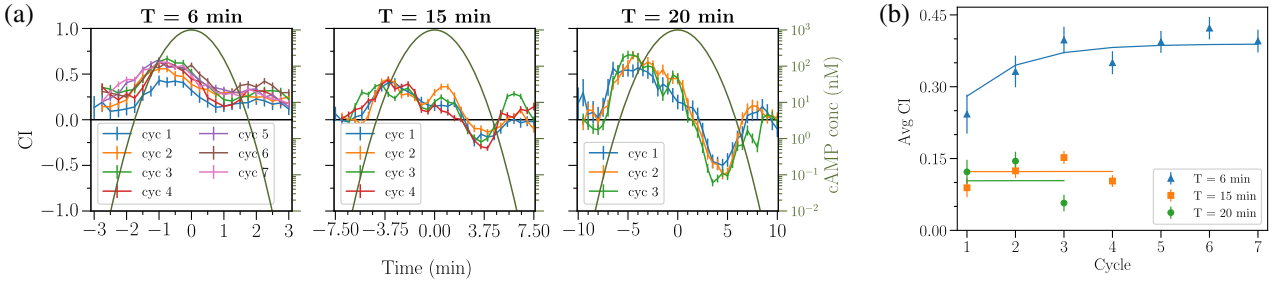


FIG. 1. (a) Chemotactic index as a function of time for time periods $T = 6$, 15, and 20 min, each with several cycles. Each data point represents the average CI of all the cells in the time bin width $\Delta t = 15$ s. Error bars represent the standard error of the mean. Also shown is the cAMP profile concentration for each wave period. (b) Average CI vs cycle number for all periods. Markers represent an average over all tracked cells and error bars represent the standard error of the mean. Lines correspond to the fits from the model.

cells respond to multiple waves, a relevant question given the aggregation process of *Dictyostelium* during which cells are exposed to numerous waves. Here, we investigate the effect of exposure to multiple waves of identical amplitude and frequency on the chemotactic ability of *Dictyostelium* cells. We show that this ability is enhanced upon exposure to multiple waves of a fast-moving wave ($T = 6$ min) and remains low and unchanged for a slow-moving wave ($T = 15$ and 20 min). Furthermore, using modeling, we show that our results support a mechanism for temporal gradient sensing and rectification.

We exposed cells of the axenic strain AX4 [35] that are developed for 5 h to multiple identical waves of cAMP with a uniform speed, generated using a microfluidic device, detailed in an earlier study [30]. In short, a cAMP stream is swept across an observation channel, resulting in a bell-shaped wave profile, similar to the one measured for natural waves of cAMP [15,36]. The wave speed can be controlled such that each wave sweeps through the substrate in a fixed time period $T$. The period was set to either 6 min (hereafter referred to as fast moving), corresponding to a physiologically relevant value [37], or to higher values, namely 15 and 20 min (hereafter referred to as slow moving). Cells were plated on a micropatterned substrate consisting of one-dimensional patterns such that cells were confined to move along only one dimension, either along or opposite the direction of wave propagation, facilitating simpler cell tracking [38]. We have shown in an earlier study that confinement of the cells does not significantly alter the chemotactic abilities of the cells [30].

Cell motion was captured by differential interference contrast microscopy and the resulting images were smoothened, segmented, and binarized. Cell tracks were constructed by identifying the nearest neighbor for each cell in the subsequent frame. Only isolated cells were considered for tracking to preclude the effects of crowding and cell contacts. We only analyzed cells that were tracked for at least two successive waves. The total number of cells tracked for each cycle and period ranged from 125 to 648. To keep the total experimentation time equivalent, we exposed cells to 7, 4, and 3 cycles of $T = 6$, 15, and 20 min, respectively. Further experimental details are presented in Supplemental Material [39].

Using the tracks, we computed a measure of the chemotactic ability of the cells called the chemotactic index (CI), defined as the ratio of the velocity of the cell in the direction of the source to the magnitude of its speed, averaged over a moving time window of length $(2\tau)$, taken to be 2 min [32]. Thus, the CI takes on values between $-1$ (motion exactly away from the source) and $+1$ (motion exactly toward the source). Since cells move only in the $x$ direction, the CI is the ratio of its displacement to its path length over the duration $2\tau$,

$$\mathrm{CI}(t) = \frac{x(t+\tau) - x(t-\tau)}{\int_{t-\tau}^{t+\tau} |dx|}. \tag{1}$$

Finally, we computed the average chemotactic index $\langle \mathrm{CI} \rangle$ for each wave cycle.

Figure 1(a) shows CI vs time data for all the wave periods and cycles used in the study. For the $T = 6$ min waves, the CI increases during the first few cycles and then saturates. In contrast, the CI for the longer wave periods remains almost unchanged for each cycle. This is also evident when we plot the average CI as a function of the wave cycle [Fig. 1(b)]: $\langle \mathrm{CI} \rangle$ increases substantially (by about 50%) for $T = 6$ min but remains roughly the same for the longer wave periods. We have verified that the increase in CI is due to an increase in the directionality of the cell motion: the (undirected) cell speed is roughly the same ($\sim$3–4 $\mu\mathrm{m\,min}^{-1}$) for all cycles and periods (Supplemental Material Fig. 1 [39]). Furthermore, the directed cell velocity displays the same trend as the average CI, as reported in an earlier study on *Dictyostelium* chemotaxis by exposing cells to multiple chemoattractant waves using a specialized microfluidic device [41] (Supplemental Material Fig. 1 [39]).

We repeated the experiments using cells that were developed for only 4 h. These cells also exhibited a significant increase in $\langle \mathrm{CI} \rangle$ for $T = 6$ min waves, similar to 5 h developed cells (Supplemental Material Fig. 2 [39]). We should note that carrying out experiments for cells that

were developed for 6 h or more was challenging since these cells displayed increased adhesion and started to clump into small aggregates. In summary, our experiments show that, in response to fast-moving waves, the chemotactic ability of cells markedly improved as the number of waves increased, independent of the development time. In contrast, for slow-moving waves, the chemotactic ability was found to be independent of the wave cycle.

We next attempted to address our experimental findings within a modeling framework. The starting point for this is our previous model, which consists of a LEGI module, together with a bistable memory module $M$ [32] [see Fig. 3(a)]. In this LEGI + $M$ model, external cAMP binds to the receptor $R$, which activates both a membrane-bound activator $E$ and a global inhibitor $I$. The membrane-bound response element $S$ of the LEGI module is activated by $E$, inhibited by $I$, and feeds into the memory module. The output of this module $M$ feeds back to $S$ and this feedback depends on $R$. This model was able to explain how cells are able to chemotax toward the wave source, even though the spatial gradient reverses direction in the back of the wave. For fast-moving waves, the memory at the front, but not the back, is activated, resulting in a continued response in the direction of the original wave [32]. The model also correctly predicted the chemotaxis of cells when a static linear gradient of the chemoattractant was reversed or when the linear gradient was switched to a uniform concentration [32]. While the LEGI model without $M$ predicts that cells remain insensitive to a falling cAMP concentration (resulting in CI = 0 in the wave back) [33], the gradient reversal experiments definitively show that cellular response goes beyond rectification, and that an additional memory component is required. Importantly, the parameter values of the LEGI and memory modules are identical to the ones used in our previous study and are listed in Supplemental Material Table 1 [39].

Here we extend the model with a new, local signaling component $X$, whose dynamics is assumed to be a function of the fraction of bound receptors $R$ and the memory module $M$ [Fig. 3(a), see Supplemental Material Sec. IV for equations [39] ]. We have considered modifying $M$ but the results were inconsistent with our experiments (see Supplemental Material Sec. IV). $X$ is a separate memory component from $M$ and operates on a different timescale. While $M$ switches between inactive and active states each cycle, the rise in the reported CI happens gradually over several cycles. This slow buildup of directional memory over several cycles is captured by $X$. Also note that $X$ is coupled to $M$ but not to either $R$, $E$, or $I$. This is because the latter model components have temporal profiles in the front vs the back that are, aside from a small time lag, identical. Thus, coupling to these variables will not result in an asymmetric response in $X$.

The model is implemented in a 1D geometry, consisting of a line (the interior of the cell) and two ends [the back ($b$) and front ($f$) of the cell]. All components, including $X$, are

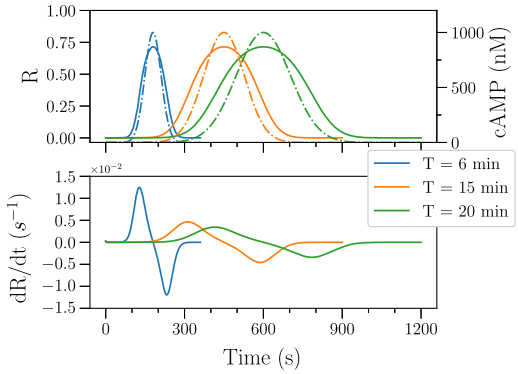


FIG. 2. Top: receptor occupancy $R$ (solid lines) and cAMP concentration (dashed lines) for different periods and for one cycle. Bottom: corresponding temporal gradient of $R$. While cAMP and $R$ have the same amplitude for all periods, the temporal gradient is greater for a fast-moving wave.

solved for at both the front and at the back, except for the global inhibitor $I$. This global component diffuses within the cell interior and its concentration is taken as uniform within the cell. Finally, the definition of CI is extended to include a contribution from $X$ in addition to $M$ and $S$: $\mathrm{CI} = \alpha(M_f - M_b) + \beta(S_f - S_b) + \gamma(X_f - X_b)$, where $\alpha$, $\beta$, and $\gamma$ are parameters that were adjusted to fit the experimental data.

In Supplemental Material Sec. IV A [39] we show that models in which $X$ is activated by the concentration of cAMP or any other downstream component, including $M$, fail to reproduce the experimental trend in the average CI. This is because cells exposed to slow-moving waves perceive high levels of $M$ for longer time than cells exposed to fast-moving waves (Fig. 2, top panel). This will lead to an elevated CI for slow-moving waves, inconsistent with our experimental findings.

Examining the profiles of $R$ experienced by cells reveals that the temporal gradient of $R$ is greater for a fast-moving wave than for a slow-moving wave (Fig. 2, bottom panel). This suggests that the response of cells may involve the temporal gradient of the $R$. Therefore, we propose that $X$ is activated only by a temporally increasing receptor occupancy $R$. Specifically, we assume that the dynamics of $X$ at the front of the cell can be written as

$$\frac{dX_f}{dt} = \frac{k_1 M_f}{1 + \exp\left[-p\left(\frac{dR_f}{dt} - \theta\right)\right]} - k_2 X_f \qquad (2)$$

with a corresponding equation for $X_b$. Here, $M$, $X$, and $R$ are the dimensionless concentrations of the components in the model with values between 0 and 1. The first term describes the activation of $X$ through a sigmoidal function of the temporal concentration $dR/dt$ of the activated receptor with a positive threshold $\theta$, which acts as a rectifier and places a lower bound on the temporal gradient

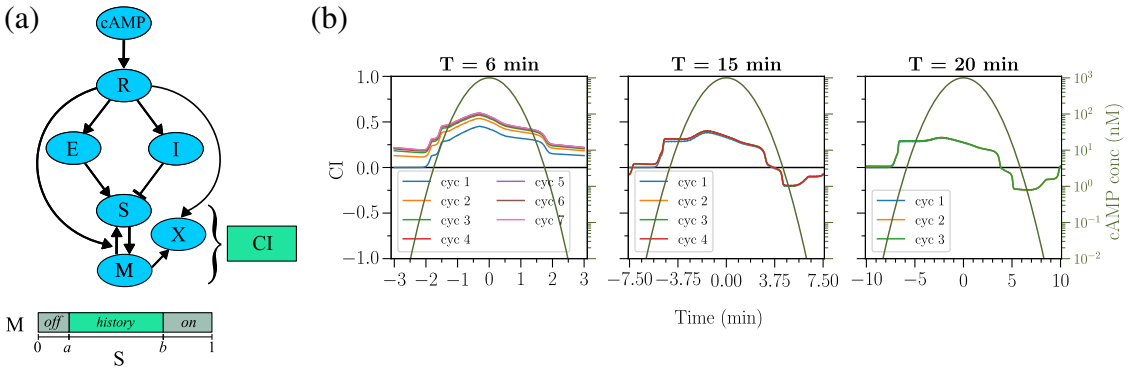


FIG. 3. (a) Schematic of the model. See Sec. IV in the Supplemental Material for equations. (b) CI vs time for multiple periods and all cycles as predicted from the model ($\alpha = \beta = \gamma = 0.15$). The plots overlap for $T = 15$ and 20 min.

for the activation of $X_f$ to occur. The parameter $p$ is a multiplicative factor that controls the steepness of the sigmoidal function. The second term describes the decay of $X_f$ following first-order kinetics.

We simulated the model shown in Fig. 3(a) for the three different wave periods with parameter values detailed in Supplemental Material [39]. The resulting CI for the different wave periods is shown in Fig. 3(b) as a function of time. Consistent with the experimental results, the CI for the fast-moving wave shows an increase for the first several cycles and then saturates. In contrast, the CI for the slow-moving waves is unchanged from one cycle to the next. The difference between the responses to fast- and slow-moving waves can be understood by examining the dynamics of $X_f - X_b$ as a function of time (Supplemental Material Fig. 3, bottom panel [39]). For the fast-moving waves, the time derivative of $R$ exceeds the threshold value $\theta$. Since the memory $M$ at the front of the cell is nonzero and is zero at the back, only the front value of $X$ increases. The decay of $X_f$ is not rapid enough to reset it to its original value, resulting in an increase of $X_f$ for the first few wave cycles, after which its mean value no longer changes. For the slow-moving waves, the time derivative does not exceed the threshold value and $X$ does not accumulate appreciably. Thus, for these periods, $X_f - X_b$ does not increase and does not contribute significantly to CI. This is also evident from the computed average CI for each cycle, shown as solid lines in Fig. 1(b). The model is able to replicate both the experimentally observed slow increase in CI data as well as the cycle-independent response for long periods.

Our experimentally observed enhancement of chemotactic ability of cells due to repeated exposure to waves has clear relevance to the aggregation of *Dictyostelium*. When waves of cAMP initially arise spontaneously from random locations, they pass through the cells in all directions; the period of these waves is usually large. Over time, the wave frequency and the cAMP concentration rise [19,37], and the center with the highest frequency or the lowest period (generally $T \sim 6$ min) dominates the rest and emits the fastest-moving waves [14]. Then, waves with a fixed direction and frequency pass through cells. At this point, enhanced chemotaxis under periodic stimulation would help cells to reach the wave center sooner. This, combined with our earlier observations that the chemotactic ability improves as the background cAMP concentration increases [30], leads to more optimal aggregation and, thus, better chances of survival.

Our proposed model has modules for both spatial and temporal gradient sensing, with the latter coupled to the former. Temporal gradient sensing is the determinant player for bacteria, which are too small and move too fast to employ spatial sensing [42]. Since eukaryotes are large enough to sense and respond to spatial gradients [43,44], most studies have focused on their response to spatial gradients. Equation (2) assumes that the temporal gradient in the receptor occupancy $dR_f/dt$ is measured instantaneously. Even when this assumption is relaxed, allowing for a lag time in the perception of the temporal gradient, we find that the results are unaffected, and that the profiles of $X$ are just shifted by the amount of lag time (Supplemental Material Fig. 4 [39]). Our study uniquely provides evidence for the dependence of chemotaxis in *Dictyostelium* on the temporal dependence of chemoattractant gradient. While the cellular response to a temporal gradient in a single wave was discussed in an earlier study [33], our Letter shows a gradual improvement in chemotactic response to fast-moving waves, driven by temporal gradient sensing. These results are consistent with a recent study, which shows that migrating myeloid cells can also sense temporal dynamics of chemoattractant concentrations [45]. Our results are also consistent with a recent study that investigated cAMP wave periods and cell movement in *Dictyostelium* populations as a function of developmental time [46]. This study showed that, as cells developed and the frequency of cAMP waves decreased, their collective cell motion and cell speed increased.

Our temporal sensing is formulated in terms of abstract variables, without specific identification of biochemical components. Such identification is challenging since a

large number of components play a role in chemotaxis [47,48] and additional studies are required to determine the exact biochemical components. We wish to reiterate the roles of the two memory components discussed here, $M$ and $X$. The presence of a feedback between the response element $S$ and the bistable memory component $M$ correctly predicts the Ras dynamics in gradient switching and reversal experiments [32] and the positive CI on the back half of the wave for fast-moving waves [30,32]. Unlike $M$, $X$ does not reset to zero after a fast-moving wave has passed. Its concentration rises gradually over several cycles upon successive activations by $M$ and temporal gradient sensing $\mathrm{d}R/\mathrm{d}t$. We have chosen the simplest functional forms for activation thresholding and decay kinetics in Eq. (2). More elaborate schemes may be possible and future work is needed to investigate this.

Our results suggest that it should be possible to further probe the temporal sensing module in future experiments. For example, if the width of the Gaussian wave profile is decreased, keeping all else equal, the magnitude of the temporal gradient increases. Our model predicts that for these narrower profiles the CI will increase as a function of cycle number, even for the slow-moving waves (Supplemental Material Fig. 5 [39]). In addition, to probe the timescale of $X$, it would be interesting to expose cells to a fast-moving wave (e.g., the wave corresponding to the $T = 6$ min period studied here) and include a pause between each successive wave. In this case, the model predicts that, during the pause, when the cells are not exposed to a cAMP signal, $X$ will decay exponentially, with a timescale governed by the decay constant $k_2$. Thus, as the pause is lengthened, $X$ will decay more, and the cycle-dependent increase of CI will become smaller. Our simulations indeed show that this increase in CI is maximal in the absence of a pause and will decrease as the pause is increased, becoming negligible if the pause exceeds 15 min (see Sec. IV and Fig. 5 in the Supplemental Material [39]). Finally, even though the biochemical nature of $X$ is not known and may involve one or more components, our model suggests specific kinetics and localization signatures. $X$ should rise and decay slowly, should be activated by the temporal gradient of cAMP concentration, and must display a front-back asymmetry in response to fast-moving waves. As such, it is possible that one or more members of the Rho family of GTPases, including Rac1, is involved in the regulation of the long term response to fast-moving waves. Clearly, a more precise identification of $X$ will necessitate further experiments.

*Acknowledgments*—A. K. thanks Mahesh Mulimani for helpful discussions and Timothy Tyree for help with software on cell tracking. We acknowledge support from by the National Science Foundation under Grants NSF DMS-1953469 and PHY-2310496.

[1] S. SenGupta, C. A. Parent, and J. E. Bear, Nat. Rev. Mol. Cell Biol. **22**, 529 (2021).
[2] F. Sallusto and M. Baggiolini, Nat. Rev. Immunol. **9**, 949 (2008).
[3] E. Scarpa and R. Mayor, J. Cell Biol. **212**, 143 (2016).
[4] E. T. Roussos, J. S. Condeelis, and A. Patsialou, Nat. Rev. Cancer **11**, 573 (2011).
[5] W. J. Rappel and W. F. Loomis, Wiley Interdiscip. Rev.: Syst. Biol. Med. **1**, 141 (2009).
[6] P. N. Devreotes, Science **245**, 1054 (1989).
[7] H. Levine and W.-J. Rappel, Phys. Today **66**, No. 2, 24 (2013).
[8] W. Roos and G. Gerisch, FEBS Lett. **68**, 170 (1976).
[9] R. H. Kessin, *Dictyostelium: The Evolution, Cell Biology, and Development of a Social Organism* (Cambridge University Press, Cambridge, England, 2001).
[10] W. F. Loomis, Dev. Biol. **391**, 1 (2014).
[11] K. Tomchik and P. N. Devreotes, Science **212**, 443 (1981).
[12] P. V. Afonso, M. Janka-Junttila, Y. J. Lee, C. P. McCann, C. M. Oliver, K. A. Aamer, W. Losert, M. T. Cicerone, and C. A. Parent, Dev. Cell **22**, 1079 (2012).
[13] T. Lämmermann, P. V. Afonso, B. R. Angermann, J. M. Wang, W. Kastenmüller, C. A. Parent, and R. N. Germain, Nature (London) **498**, 371 (2013).
[14] K. J. Lee, E. C. Cox, and R. E. Goldstein, Phys. Rev. Lett. **76**, 1174 (1996).
[15] P. N. Devreotes, M. J. Potel, and S. A. MacKay, Dev. Biol. **96**, 405 (1983).
[16] J. J. Tyson, K. A. Alexander, V. Manoranjan, and J. Murray, Physica (Amsterdam) **34D**, 193 (1989).
[17] T. Höfer, J. A. Sherratt, and P. K. Maini, Physica (Amsterdam) **85D**, 425 (1995).
[18] H. Levine, I. Aranson, L. Tsimring, and T. V. Truong, Proc. Natl. Acad. Sci. U.S.A. **93**, 6382 (1996).
[19] J. Noorbakhsh, D. J. Schwab, A. E. Sgro, T. Gregor, and P. Mehta, Phys. Rev. E **91**, 062711 (2015).
[20] A. Levchenko and P. A. Iglesias, Biophys. J. **82**, 50 (2002).
[21] H. Levine, D. A. Kessler, and W. J. Rappel, Proc. Natl. Acad. Sci. U.S.A. **103**, 9761 (2006).
[22] P. A. Iglesias and P. N. Devreotes, Curr. Opin. Cell Biol. **20**, 35 (2008).
[23] P. J. V. Haastert and P. N. Devreotes, Nat. Rev. Mol. Cell Biol. **5**, 626 (2004).
[24] K. F. Swaney, C. H. Huang, and P. N. Devreotes, Annu. Rev. Biophys. **39**, 265 (2010).
[25] S. K. Dertinger, D. T. Chiu, S. K. Dertinger, and G. M. Whitesides, Anal. Chem. **73**, 1240 (2001).
[26] D. Fuller, W. Chen, M. Adler, A. Groisman, H. Levine, W. J. Rappel, and W. F. Loomis, Proc. Natl. Acad. Sci. U.S.A. **107**, 9656 (2010).
[27] C. Beta and E. Bodenschatz, Eur. J. Cell Biol. **90**, 811 (2011).
[28] B. Hamza, E. Wong, S. Patel, H. Cho, J. Martel, and D. Irimia, Integr. Biol. **6**, 175 (2014).
[29] M. A. Qasaimeh, M. Pyzik, M. Astolfi, S. M. Vidal, and D. Juncker, Adv. Biosyst. **2**, 1700243 (2018).
[30] R. Karmakar, M.-H. Tang, H. Yue, D. Lombardo, A. Karanam, B. A. Camley, A. Groisman, and W.-J. Rappel, Phys. Rev. E **103**, 012402 (2021).

[31] K. Takeda, D. Shao, M. Adler, P. G. Charest, W. F. Loomis, H. Levine, A. Groisman, W.-J. Rappel, and R. A. Firtel, Sci. Signal. (Online) **5**, ra2 (2012).
[32] M. Skoge, H. Yue, M. Erickstad, A. Bae, H. Levine, A. Groisman, W. F. Loomis, and W.-J. Rappel, Proc. Natl. Acad. Sci. U.S.A. **111**, 14448 (2014).
[33] A. Nakajima, S. Ishihara, D. Imoto, and S. Sawai, Nat. Commun. **5**, 5367 (2014).
[34] C. A. Parent and P. N. Devreotes, Science **284**, 765 (1999).
[35] M. Sussman, in *Methods in Cell Biology* (Elsevier, New York, 1987), Vol. 28, pp. 9–29.
[36] M. Postma and P. J. van Haastert, in *Chemotaxis* (Springer, New York, 2009), pp. 473–488.
[37] T. Gregor, K. Fujimoto, N. Masaki, and S. Sawai, Science **328**, 1021 (2010).
[38] R. Karmakar, C. Schich, N. Kamprad, V. Scheller, E. Gutierrez, A. Groisman, W.-J. Rappel, and M. Tarantola, PLoS One **15**, e0236171 (2020).
[39] See Supplemental Material at http://link.aps.org/supplemental/10.1103/PhysRevLett.133.068401, which includes Ref. [40], for additional experimental details and an extended discussion of the model.
[40] R. Karmakar, T. Tyree, R. H. Gomer, and W.-J. Rappel, Proc. Natl. Acad. Sci. U.S.A. **118** (2021).
[41] A. Nakajima, M. Ishida, T. Fujimori, Y. Wakamoto, and S. Sawai, Lab Chip **16**, 4382 (2016).
[42] V. Sourjik and N. S. Wingreen, Curr. Opin. Cell Biol. **24**, 262 (2012).
[43] L. Song, S. M. Nadkarni, H. U. Bödeker, C. Beta, A. Bae, C. Franck, W.-J. Rappel, W. F. Loomis, and E. Bodenschatz, Eur. J. Cell Biol. **85**, 981 (2006).
[44] P. J. van Haastert and M. Postma, Biophys. J. **93**, 1787 (2007).
[45] C. E. P. Aronin, Y. M. Zhao, J. S. Yoon, N. Y. Morgan, T. Prüstel, R. N. Germain, and M. Meier-Schellersheim, Immunity **47**, 862 (2017).
[46] H. Z. Ford, A. Manhart, and J. R. Chubb, eLife **12**, e83796 (2023).
[47] P. N. Devreotes, S. Bhattacharya, M. Edwards, P. A. Iglesias, T. Lampert, and Y. Miao, Annu. Rev. Cell Dev. Biol. **33**, 103 (2017).
[48] X. Li, Y. Miao, D. S. Pal, and P. N. Devreotes, in *Seminars in Cell & Developmental Biology* (Elsevier, New York, 2020), Vol. 100, pp. 133–142.